Hybrid III-V semiconductor/silicon nanolaser

Y. Halioua,[1,2] A. Bazin,[1] P. Monnier,[1] T. J. Karle,[1] G. Roelkens,[2] I. Sagnes,[1] R. Raj,[1] and F. Raineri[1,3,*]

[1]*Laboratoire de Photonique et de Nanostructures, CNRS-UPR20, Route de Nozay, 91460 Marcoussis, France*
[2]*Photonics Research Group, Department of Information Technology, Ghent University, B-9000 Ghent, Belgium*
[3]*Université Paris Denis Diderot, 75205 Paris, France*
**fabrice.raineri@lpn.cnrs.fr*

Abstract: Heterogeneous integration of III-V compound semiconductors on Silicon on Insulator is one the key technology for next-generation on-chip optical interconnects. In this context, the use of photonic crystals lasers represents a disruptive solution in terms of footprint, activation energy and ultrafast response. In this work, we propose and fabricate very compact laser sources integrated with a passive silicon waveguide circuitry. Using a subjacent Silicon-On-Insulator waveguide, the emitted light from a photonic crystal based cavity laser is efficiently captured. We study experimentally the evanescent wave coupling responsible for the funneling of the emitted light into the silicon waveguide mode as a function of the hybrid structure parameters, showing that 90% of coupling efficiency is possible.

OCIS codes: (230.5298) Photonic crystals; (140.3460) Lasers.

References and links

1. M. J. Kobrinsky, B. A. Block, J.-F. Zheng, B. C. Barnett, E. Mohammed, M. Reshotko, F. Robertson, S. List, I. Young, and K. Cadien, "On-chip optical interconnects," Intel Technol. J. **8**, 129–141 (2004).
2. G. Roelkens, L. Liu, D. Liang, R. Jones, A. Fang, B. Koch, and J. Bowers, "III-V/silicon photonics for on-chip and inter-chip optical interconnects," Laser Photonics Rev. **4**(6), 751–779 (2010).
3. D. A. B. Miller, "Physical reasons for optical interconnection," Int. J. Optoelectron. **11**, 155–168 (1997).
4. P. Dumon, W. Bogaerts, V. Wiaux, J. Wouters, S. Beckx, J. Van Campenhout, D. Taillaert, B. Luyssaert, P. Bienstman, D. Van Thourhout, and R. Baets, "Low-loss SOI photonic wires and ring resonators fabricated with deep UV lithography," IEEE Photon. Technol. Lett. **16**(5), 1328–1330 (2004).
5. Y. Vlasov and S. McNab, "Losses in single-mode silicon-on-insulator strip waveguides and bends," Opt. Express **12**(8), 1622–1631 (2004).
6. A. W. Fang, H. Park, O. Cohen, R. Jones, M. J. Paniccia, and J. E. Bowers, "Electrically pumped hybrid AlGaInAs-silicon evanescent laser," Opt. Express **14**(20), 9203–9210 (2006).
7. J. Van Campenhout, P. Rojo Romeo, P. Regreny, C. Seassal, D. Van Thourhout, S. Verstuyft, L. Di Cioccio, J.-M. Fedeli, C. Lagahe, and R. Baets, "Electrically pumped InP-based microdisk lasers integrated with a nanophotonic silicon-on-insulator waveguide circuit," Opt. Express **15**(11), 6744–6749 (2007).
8. A. W. Fang, E. Lively, Y.-H. Kuo, D. Liang, and J. E. Bowers, "A distributed feedback silicon evanescent laser," Opt. Express **16**(7), 4413–4419 (2008).
9. T. Dupont, L. Grenouillet, A. Chelnokov, and P. Viktorovitch, "Contradirectional coupling between III-V stacks and silicon-on-insulator corrugated waveguides for laser emission by distributed feedback effect," IEEE Photon. Technol. Lett. **22**(19), 1413–1415 (2010).
10. H. Park, A. W. Fang, O. Cohen, R. Jones, M. J. Paniccia, and J. E. Bowers, "A hybrid AlGaInAs–silicon evanescent amplifier," IEEE Photon. Technol. Lett. **19**(4), 230–2232 (2007).
11. H.-W. Chen, Y.-H. Kuo, and J. E. Bowers, "High speed hybrid silicon evanescent Mach-Zehnder modulator and switch," Opt. Express **16**(25), 20571–20576 (2008).
12. L. Liu, J. Van Campenhout, G. Roelkens, A. Soref, D. Van Thourhout, P. Rojo-Romeo, P. Regreny, C. Seassal, J.-M. Fédéli, and R. Baets, "Carrier-injection-based electro-optic modulator on silicon-on-insulator with a heterogeneously integrated III-V microdisk cavity," Opt. Lett. **33**(21), 2518–2520 (2008).
13. L. Liu, R. Kumar, K. Huybrechts, T. Spuesens, G. Roelkens, E.-J. Geluk, T. de Vries, P. Regreny, D. Van Thourhout, R. Baets, and G. Morthier, "An ultra-small, low-power, all-optical flip-flop memory on a silicon chip," Nat. Photonics **4**(3), 182–187 (2010).
14. H. A. Haus, *Waves and Fields in Optoelectronics* (Prentice-Hall, 1984).
15. P. R. Villeneuve, J. S. Foresi, J. Ferrera, E. R. Thoen, G. Steinmeyer, S. Fan, J. D. Joannopoulos, L. C. Kimerling, H. I. Smith, and E. P. Ippen, "Photonic-bandgap microcavities in optical waveguides," Nature **390**(6656), 143–145 (1997).

#144421 - $15.00 USD Received 18 Mar 2011; revised 19 Apr 2011; accepted 19 Apr 2011; published 26 Apr 2011

16. A. R. Md Zain, N. P. Johnson, M. Sorel, and R. M. De La Rue, "Ultra high quality factor one dimensional photonic crystal/photonic wire micro-cavities in silicon-on-insulator (SOI)," Opt. Express **16**(16), 12084–12089 (2008).
17. M. Notomi, E. Kuramochi, and H. Taniyama, "Ultrahigh-Q nanocavity with 1D photonic gap," Opt. Express **16**(15), 11095–11102 (2008).
18. P. B. Deotare, M. W. McCutcheon, I. W. Frank, M. Khan, and M. Lončar, "High quality factor photonic crystal nanobeam cavities," Appl. Phys. Lett. **94**(12), 121106 (2009).
19. Y. Zhang, M. Khan, Y. Huang, J. Ryou, P. Deotare, R. Dupuis, and M. Lončar, "Photonic crystal nanobeam lasers," Appl. Phys. Lett. **97**(5), 051104 (2010).
20. B. H. Ahn, J.-H. Kang, M.-K. Kim, J.-H. Song, B. Min, K.-S. Kim, and Y.-H. Lee, "One-dimensional parabolic-beam photonic crystal laser," Opt. Express **18**(6), 5654–5660 (2010).
21. Y. Halioua, A. Bazin, P. Monnier, T. J. Karle, I. Sagnes, G. Roelkens, D. Van Thourhout, F. Raineri, and R. Raj, "III-V photonic crystal wire cavity laser on silicon wafer," J. Opt. Soc. Am. B **27**(10), 2146–2150 (2010).
22. P. Velha, J. C. Rodier, P. Lalanne, J. P. Hugonin, D. Peyrade, E. Picard, T. Charvolin, and E. Hadji, "Ultra-high-reflectivity photonic-bandgap mirrors in a ridge SOI waveguide," N. J. Phys. **8**(9), 204 (2006).
23. B.-S. Song, S. Noda, T. Asano, and Y. Akahane, "Ultra-high-Q photonic double-heterostructure nanocavity," Nat. Mater. **4**(3), 207–210 (2005).
24. D. Taillaert, F. Van Laere, M. Ayre, W. Bogaerts, D. Van Thourhout, P. Bienstman, and R. Baets, "Grating couplers for coupling between optical fibers and nanophotonic waveguides," Jpn. J. Appl. Phys. **45**(No. 8A), 6071–6077 (2006).
25. T. J. Karle, Y. Halioua, F. Raineri, P. Monnier, R. Braive, L. Le Gratiet, G. Beaudoin, I. Sagnes, G. Roelkens, F. van Laere, D. Van Thourhout, and R. Raj, "Heterogeneous integration and precise alignment of InP-based photonic crystal lasers to complementary metal-oxide semiconductor fabricated silicon-on-insulator wire waveguides," J. Appl. Phys. **107**(6), 063103 (2010).
26. G. Bjork and Y. Yamamoto, "Analysis of semiconductor microcavity lasers using rate equations," IEEE J. Quantum Electron. **27**(11), 2386–2396 (1991).
27. E. Kapon, *Semiconductor Lasers* (Academic Press, 1999).
28. W. Suh, Z. Wang, and S. Fan, "Temporal coupled-mode theory and the presence of non orthogonal modes in lossless multimode cavities," IEEE J. Quantum Electron. **40**(10), 1511–1518 (2004).
29. C. Manolatou, M. J. Khan, S. Fan, P. R. Villeneuve, H. A. Haus, and J. D. Joannopoulos, "Coupling of modes analysis of resonant channel add–drop filters," IEEE J. Quantum Electron. **35**(9), 1322–1331 (1999).
30. Y. Dumeige, S. Trebaol, L. Ghişa, T. K. Nguyên, H. Tavernier, and P. Féron, "Determination of coupling regime of high-Q resonators and optical gain of highly selective amplifiers," J. Opt. Soc. Am. B **25**(12), 2073–2110 (2008).
31. W.-P. Huang, "Coupled-mode theory for optical waveguides: an overwiew," J. Opt. Soc. Am. A **11**(3), 963–983 (1994).
32. P. S. Zory, *Quantum Well Lasers* (Academic, 1993).
33. H. Kawaguchi, "Optical bistability and chaos in a semiconductor laser with saturable absorber," Appl. Phys. Lett. **45**(12), 1264–1266 (1984).
34. F. Raineri, C. Cojocaru, P. Monnier, A. Levenson, R. Raj, C. Seassal, X. Letartre, and P. Viktorovitch, "Ultrafast dynamics of the third-order nonlinear response in a two-dimensional InP-based photonic crystal," Appl. Phys. Lett. **85**(11), 1880–1882 (2004).
35. H. Altug, D. Englund, and J. Vuckovic, "Ultrafast photonic crystal nanocavity laser," Nat. Phys. **2**(7), 484–488 (2006).
36. E. Rosencher and B. Vinter, *Optoelectronics* (Cambridge University Press, 2002).
37. P. E. Barclay, K. Srinivasan, and O. Painter, "Design of photonic crystal waveguides for evanescent coupling to optical fiber tapers and integration with high-*Q* cavities," J. Opt. Soc. Am. B **20**(11), 2274–2284 (2003).
38. I.-K. Hwang, S.-K. Kim, J.-K. Yang, S.-H. Kim, S. H. Lee, and Y.-H. Lee, "Curved-microfiber photon coupling for photonic crystal light emitter," Appl. Phys. Lett. **87**(13), 131107 (2005).
39. K. Nozaki, H. Watanabe, and T. Baba, "Photonic crystal nanolaser monolithically integrated with passive waveguide for effective light extraction," Appl. Phys. Lett. **92**(2), 021108 (2008).
40. S. Matsuo, A. Shinya, T. Kakitsuka, K. Nozaki, T. Segawa, T. Sato, Y. Kawaguchi, and M. Notomi, "High-speed ultracompact buried heterostructure photonic-crystal laser with 13fJ of energy consumed per bit tranjsmitted," Nat. Photonics **4**(9), 648–654 (2010).
41. B. Ellis, T. Sarmiento, M. Mayer, B. Zhang, J. Harris, E. Haller, and J. Vuckovic, "Electrically pumped photonic crystal nanocavity light sources using a laterally doped p-i-n junction," Appl. Phys. Lett. **96**(18), 181103 (2010).
42. H.-G. Park, S.-H. Kim, S.-H. Kwon, Y.-G. Ju, J.-K. Yang, J.-H. Baek, S.-B. Kim, and Y.-H. Lee, "Electrically driven single-cell photonic crystal laser," Science **305**(5689), 1444–1447 (2004).

1. Introduction

During the past decades, optical devices have come to play a crucial role in the domain of information and communication technology, by delivering high bandwidth solutions to long-haul data transmission. Increasing attention is now devoted to optical computer-com mainly concentrated in intra- and inter-chip interconnection applications [1,2], the convergence of optics and electronics at the chip level being a necessity for the next generation processors.

#144421 - $15.00 USD Received 18 Mar 2011; revised 19 Apr 2011; accepted 19 Apr 2011; published 26 Apr 2011

Here, the issues that need to be tackled are the rapid dispatching and sorting of the mind-boggling amounts of information within small footprints and above all with reduced power consumption [3].

Thus, photonic circuits should be built from elements able to perfectly control the propagation of light to achieve "passive" functions such as guiding and filtering as well as elements dedicated to active functions such as emission, detection, amplification, switching and a multitude of others capable to manipulate optical information at will.

It is very unlikely that only one class of material will completely respond to all needs. Silicon photonics, enhanced by III-V based optical functions is considered to be as one of the key technologies combining the best of both materials leading to a highly versatile hybrid photonics platform which opens the way to large scale photonic integration. Indeed, silicon's transparency at telecom wavelengths and its high-index contrast with silica allows the fabrication of extremely compact low-loss single mode waveguides (~2dB/cm) [4,5] that can be used to route information through a circuit. Critically, the mature complementary metal oxide semiconductor (CMOS) fabrication processing technology renders possible large-scale integration of functional optical devices, including integration with complex electronic components. However, due to its indirect electronic band gap Silicon is not the most ideal material for light emission and light control. The direct bandgap of III-V materials makes efficient stimulated emission possible, which enables the fabrication of lasers, amplifiers, detectors and modulators. These materials permit to obtain tailor-made electronic band structures by engineering their composition to form suitable alloys. Radiative transitions can thus be obtained at the desired wavelength, ranging from 0.4μm to 20μm. Heterogeneous integration of III-V semiconductors on Silicon on Insulator (SOI) waveguides has recently succeeded in the realization of laser sources [6–9], amplifiers [10], modulators [11,12] and flip-flops [13], all of them very exciting results for further photonic integration with electronics.

In this article, the concept of hybrid Si/III-V semiconductor photonics is scaled down to nanophotonics. III-V Photonic crystal nanolasers are integrated with and coupled to SOI waveguides circuitry. This disruptive approach allows us to obtain low threshold hybrid lasers in the telecom window within a footprint as small as $5\mu m^2$, ten times smaller than the smallest microdisks devices demonstrated so far. We experimentally study the evanescent wave coupling in the device as a function of the structure parameters and show that more than 90% of the emitted light is funneled into the SOI wires.

2. An innovative platform: hybrid III-V photonic crystals nanocavities on silicon on insulator waveguides circuitry

The hybrid structure under study is schematically represented on Fig. 1a. It is a 2 optical level structure where one level is constituted by a single mode SOI wire waveguide and the other, an InP-based photonic crystal nanocavity with 4 InGaAsP/InGaAs quantum wells embedded which emit at 1.55μm. The 2 levels are separated by a low index layer (silica + benzocyclobutene) which preserve the vertical optical confinement within the SOI waveguide and the PhC cavity. Coupling is ensured by the penetration the evanescent tail of the optical modes into the other level [14].

The chosen nanocavity is akin to a "wire" or "nanobeam" [15–21] cavity, which is a Fabry-Perot type cavity formed in a single mode wire waveguide (550nm width and 255nm height). High reflectivity mirrors are constituted by a single row of holes drilled into the material. The holes diameter d and the pitch of the 1D lattice a are fixed to be respectively at 177.5nm and 370 nm to obtain a large high reflectivity bandwidth around 1.55μm. The sizes of the 3 holes on each side of the cavity are tapered down in order to increase the quality factor by adapting the propagating guided mode to the evanescent mirror mode [22].

#144421 - $15.00 USD Received 18 Mar 2011; revised 19 Apr 2011; accepted 19 Apr 2011; published 26 Apr 2011

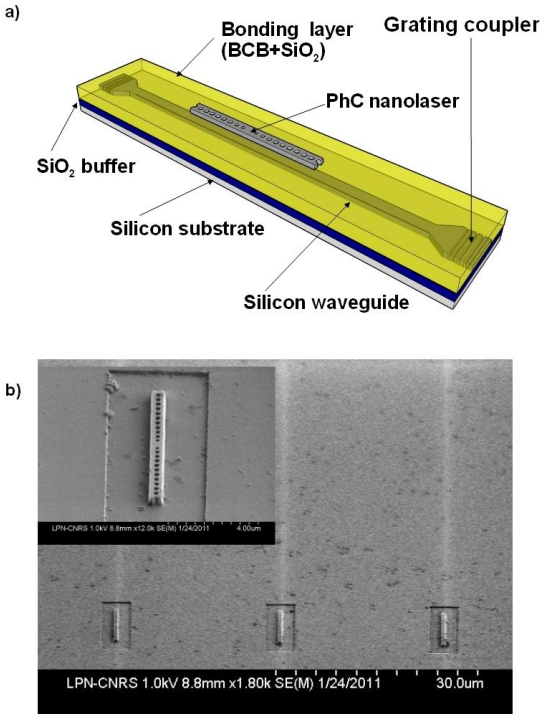

Fig. 1. Hybrid III-V Semiconductor Photonic Crystal on SOI waveguide circuitry. a) Schematic view of the structure. The InP-based photonic-crystal wire cavity nanolaser is positioned on top of silicon on insulator strip waveguide. The 2 structures are separated by a low-refractive index bonding layer constituted of BCB and SiO_2. b) SEM images of the fabricated sample. The SOI waveguides can be seen through the bonding layer aligned with the cavities. Inset: SEM image close-up of a wire cavity.

These cavities are particularly interesting because they can exhibit quality factors as high as 10^5 with modal volumes close to the limit of $(\lambda/2n)^3$ even when the structures are not suspended in air, as is the case in the present study. Moreover, their total length varying from 8.3µm to 8.55µm, their footprint is about $5\mu m^2$, which is at least 10 times smaller than the footprint of cavities formed in a 2 dimensional lattice of holes [23]. The SOI level is made of a 220nm thick Si layer on a 2µm SiO_2 buffer. The Si layer is etched down in order to form waveguides of widths varying from 300nm to 550nm in steps of 50nm. Grating couplers are etched at a distance from the circuitry to allow coupling with cleaved single mode optical fibres [24]. The fabrication of the hybrid structures relies on the adhesive bonding using Benzocyclobutene (BCB). The InP-based heterostructure, containing 4 InGaAs/InGaAsP quantum wells is grown by metalorganic vapour phase epitaxy (MOVPE), the SOI waveguides being processed on a CMOS pilot-line. A 300nm thick layer of BCB is spun onto the SOI wafer surface in order to planarize the surface and leave 80nm of polymer above the Si waveguides. The InP wafer is sputter coated with a SiO_2 layer whose thickness is chosen to be either 200nm, 300nm or 400nm before being put in contact with the BCB coated SOI wafer. The sample is then pressed and cured for 3 hours at 300°C under N_2 atmosphere to finalize the bonding. After the chemical removal of the InP substrate, the PhC cavities are patterned on the active membrane using inductively coupled plasma etching through a silicon nitride mask. The latter is obtained by positive electron beam lithography followed by reactive ion etching. A 30nm-precise alignment of the III-V nanocavities to the SOI waveguides is achieved using, during the electron beam lithography, reference markers fabricated in the silicon waveguide level. After the silicon nitride mask removal, the excess InP-based membrane left on the surface is chemically etched away while protecting the nanocavities

#144421 - $15.00 USD Received 18 Mar 2011; revised 19 Apr 2011; accepted 19 Apr 2011; published 26 Apr 2011

with negative electron beam lithography resist. More details on the fabrication can be found in references [25].

The low index layer below the cavity is a bilayer composed of a thin layer of BCB (80nm) and a layer of SiO_2. Compared to a low-n layer only composed of BCB, this configuration enables a better control on the InP-SOI separation but also an improvement in the thermal dissipation of the laser as SiO_2 thermal conductivity is 3 times greater than the BCB thermal conductivity. A scanning electron microscope picture of one of the fabricated structures is given on Fig. 1b where a wire cavity can be seen positioned on top of a SOI waveguide.

3. Laser operation

Laser emission is explored at room temperature by optically surface pumping the wire cavities using an 800nm laser diode focused to a 20 μm^2 spot by a 10x microscope objective. The laser diode is modulated in order to obtain 40ns pulses at a 300kHz repetition rate. The emitted light is collected via the gratings at the extremities of the 8mm long SOI waveguides with SMF-28 optical fibres tilted at an angle of 10° to the surface normal and is analysed using a spectrometer equipped with a cooled InGaAs detector array.

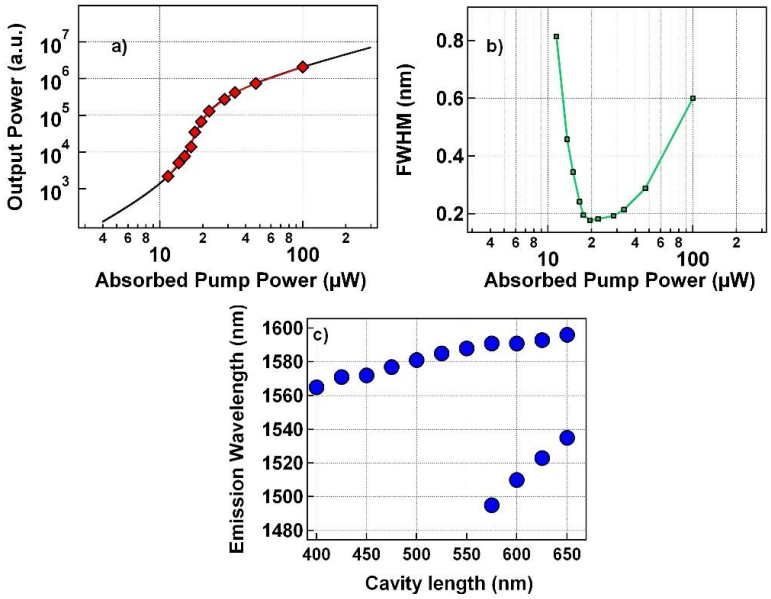

Fig. 2. Experimental PhC wire cavity nanolaser emission characteristic curves. a) Intensity of the emitted light outputting the SOI waveguide as a function the absorbed pump power. The black line is a fit of the experimental data using the rate equations for quantum well lasers given in the text. b) Full width at half maximum of the emission spectral linewidth as a function of the absorbed pump power. c) Emission wavelength as a function of the cavity length, i.e. centre to centre distance between the first 2 tapered holes.

We plot in Fig. 2a, in log-log scale, the output peak power of the emitted light as a function of the absorbed pump peak power for a 450nm-long cavity coupled to a 500nm wide SOI waveguide (SiO_2 thickness is 400nm). Here, we estimate the amount of absorbed pump power in the III-V layer by taking into account the material absorption (30% in 255nm), the reflectivity at the interfaces (30% at the interface) and the ratio of the cavity surface and the pump spot size (4%). As expected for laser emission [26], the curve is S-shaped, with a threshold of 17μW (total peak power 2mW). As seen in Fig. 2b, the full width at half maximum (FWHM) of the emission spectrum decreases to 0.18nm (corresponding to the spectrometer resolution) as the absorbed pump power is increased up to 19.5μW. When the pump power is further increased the emission broadens due to power broadening [27]. The emission wavelength can be easily tuned by adjusting, for example, the cavity length as

#144421 - $15.00 USD Received 18 Mar 2011; revised 19 Apr 2011; accepted 19 Apr 2011; published 26 Apr 2011

shown in Fig. 2c [21]. As the cavity length is increased from 400nm to 650nm, the cavities remain single mode and laser emission is observed in the range 1565nm to 1596nm. Above 550nm, 2 peaks are observed in the emission spectra as the cavity second order mode enters the gain bandwidth of the QWs. In the following, we will focus on the single mode cavities.

4. Study of the coupling efficiency

One important question remains which has not been addressed experimentally in the hybrid systems: what is the efficiency of the coupling between the III-V nanolaser and the SOI wire? In the approximation where the presence of the SOI waveguide weakly perturbs the cavity mode, the evolution of the intra-cavity electromagnetic field can be described by the coupled-mode theory (CMT) [28–30]. In this theory, the cavity optical losses are determined by two independent terms, one related to the intrinsic losses of the cavity, i.e. the losses in absence of the waveguide and one related to the coupling to the SOI waveguide mode [31]. These are described respectively by the quality factors Q_0 and Q_c.

The coupling efficiency can then be written as:

$$\eta = \frac{\frac{1}{Q_c}}{\frac{1}{Q_c}+\frac{1}{Q_0}}$$

It is clear that, in order to obtain a large efficiency, the coupling losses must be much larger than the intrinsic cavity losses ($Q_c << Q_0$). The coupling efficiency is plotted in Fig. 3a as a function of the ratio Q_0/Q_c. At the same time, the total losses of the system (proportional to $1/Q_0 + 1/Q_c$) must be maintained as small as possible to allow low threshold laser emission. Q_c and Q_0 can be experimentally retrieved by analysing the transmission of an optical probe as a function of the material gain and the laser characteristic in tandem.

In our active hybrid system, the evolution of the intra cavity field amplitude E_{cav} in the presence of optical gain is derived from the CMT and reads:

$$\frac{dE_{cav}}{dt} = \left(j\omega_0 - \frac{1}{\tau_0} - \frac{1}{\tau_c} + \frac{1}{\tau_g} \right) E_{cav} + \sqrt{\frac{1}{\tau_c}}\varepsilon_{in}$$

Where $|E_{cav}|^2$ is the energy in the cavity mode, $|\varepsilon_{in}|^2$ is the power in the SOI waveguide mode incident upon the cavity (Fig. 3b), ω_0 is the field pulsation at resonance, $1/\tau_g$ is the term related to the optical gain and $\tau_{0,c} = 2Q_{0,c}/\omega_0$ is the time constant associated to the intrinsic/coupling losses. When the gain medium is composed of QWs embedded in a semiconductor slab, this term depends on the carrier density [32] as: $1/\tau_g = \Gamma \sigma v_g (N - N_{tr})/2$ with Γ the confinement factor, σ the differential gain, v_g the optical group velocity and N_{tr} the carrier density at transparency. The transmission can then be expressed as:

$$T(\omega) = \left| 1 - \frac{\frac{1}{\tau_c}}{j(\omega - \omega_0) + \frac{1}{\tau_c} + \frac{1}{\tau_0} - \frac{1}{\tau_g}} \right|^2$$

Figure 3c shows the theoretical transmission at resonance $T(\omega_0)$ as a function of $1/\tau_g$ for Q_0 = 10000 and Q_c = 2000, i.e. with a ratio Q_0/Q_c of 5. When $1/\tau_g$ is negative, the material is

#144421 - $15.00 USD Received 18 Mar 2011; revised 19 Apr 2011; accepted 19 Apr 2011; published 26 Apr 2011

absorptive and the transmission stays close to 1. As $1/\tau_g$ is increased and becomes positive, the transmission diminishes and becomes zero when the gain exactly balances the intrinsic losses of the cavity ($1/\tau_g = 1/\tau_0$). At this gain, the total cavity losses are determined by the coupling to the SOI waveguide and Q_c can be directly obtained by measuring the FWHM of the resonance in the transmission spectrum.

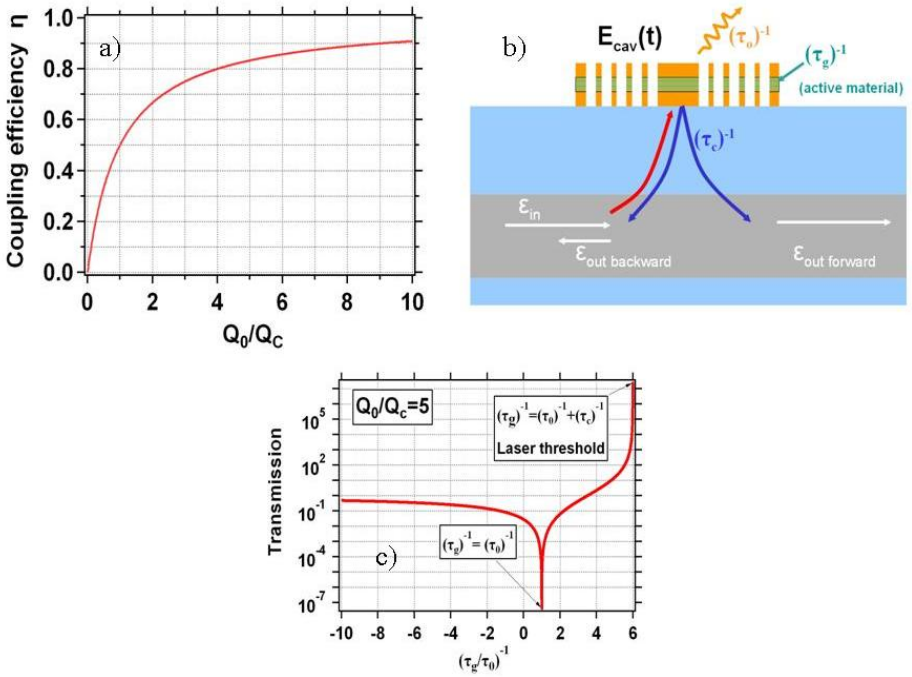

Fig. 3. Coupling model. a) Theoretical coupling efficiency as a function of the ratio Q_0/Q_c . b) Schematics of the system considered for the couple mode theory. An incoming field E_{in} in the SOI waveguide is coupled to a single mode cavity via evanescent wave coupling. The intracavity field is denoted E_{cav} and the transmitted field in the forward direction $E_{out\ forward}$. $(\tau_0)^{-1}$ and $(\tau_c)^{-1}$ are the inverse of the time constants corresponding to the intrinsic losses of the cavity and to the coupling between the cavity and the waveguide. The presence of the active material in the cavity is taken into account by adding an extra characteristic time constant τ_g which depends on the absorbtion/gain of the material. c) Theoretical transmission at resonance as a function of $(\tau_g/\tau_0)^{-1}$ for $Q_0/Q_c = 5$ obtained with couple mode theory.

When $1/\tau_g$ is further increased, net amplification is observed for $1/\tau_g > 1/\tau_0 + 1/2\tau_c$ and the lasing threshold is reached when $1/\tau_g = 1/\tau_0 + 1/\tau_c$ (gain compensates all losses).

Pump-probe experiments are performed to measure the variation of the transmission spectrum around the cavity resonance wavelength as a function of the material gain. The pump, delivered at 800nm as above controls the gain of the active material. A modulated tunable laser source around 1.55 µm (13ns pulses at 300kHz repetition rate) is injected in the SOI waveguide and used as the probe. An extra 5kHz modulation is applied to the probe to discriminate the probe signal from the emission via homodyne detection.

The measured transmission spectra are plotted in Fig. 4a as a function of the absorbed pump power for a 450nm-long cavity coupled to a 350nm wide waveguide (SiO_2 thickness is 300nm). Firstly, the transmission shows a dip at resonance which deepens with increasing pump power reaching a minimum at $\lambda = 1550$nm when $P_{pump} = P_0 = 12.4$µW. Net amplification is then observed before attaining the laser emission at a threshold of 29.6µW for this particular sample. As the material refractive index is dependent on the carrier density, the change in amplitude is also accompanied by a blue-shift of the resonant wavelength. This is

#144421 - $15.00 USD Received 18 Mar 2011; revised 19 Apr 2011; accepted 19 Apr 2011; published 26 Apr 2011

nominally clamped when the laser threshold is reached. The good qualitative agreement of these measurements with modelling can be appreciated in Fig. 4b, where the transmission at resonance is plotted as a function of the absorbed pump power. The FWHM of the resonance is measured to be 0.83nm at $P = P_0$ giving $Q_c = 1800$ (see Fig. 4c).

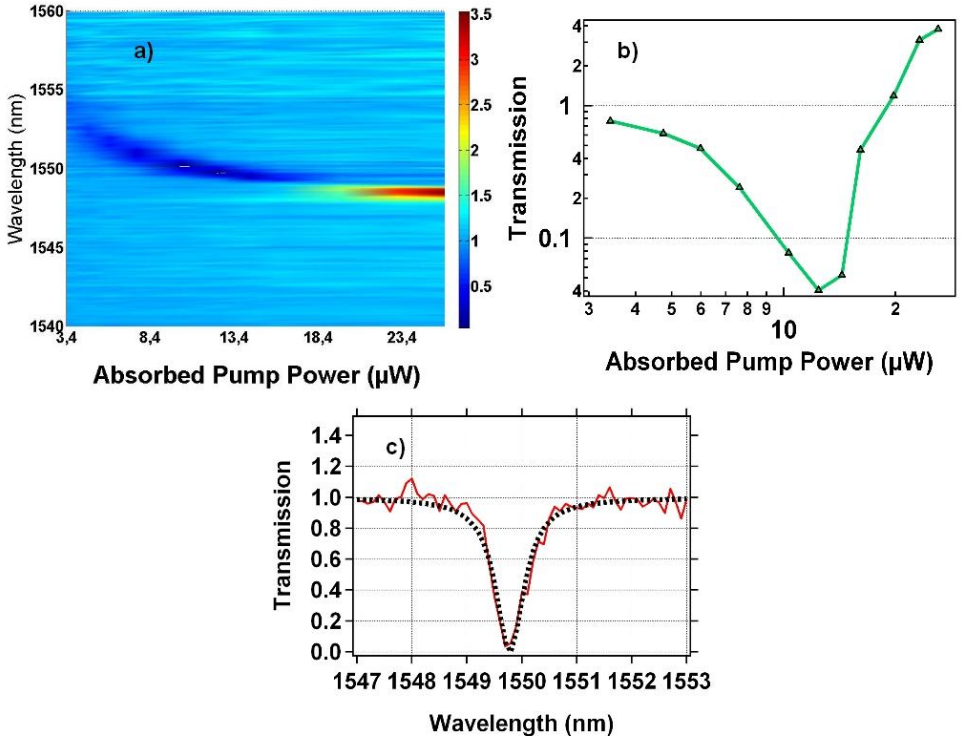

Fig. 4. Transmission measurements. a) Transmission spectra of the coupled system as a function of the absorbed pump power.. b) Transmission at resonance as a function of the pump power, these values corresponding to transmission minimum/maximum when the spectra exhibit a dip/peak. c) Transmission spectrum obtained with a 12.4μW pump power corresponding to the case when $\tau_g = \tau_0$ giving the minimum of transmission at resonance. The fitting of the curve using a lorentzian lineshape gives a FWHM of 0.83nm.

These measurements are repeated on samples with low-n layers of different thicknesses (z) and Si waveguides of different widths (w). In order to evaluate the impact of these structural parameters on the evanescent wave coupling, the measured Q_c are plotted on Fig. 5a. As expected from theory [31], Q_c strongly increases with z for a fixed value of w as the evanescent tail of the field of each level rapidly decays with the distance. As w is varied, Q_c varies from 5000 to 32000, from 1500 to 7800, and from 1400 to 3700 for z = 400nm, z = 300nm, z = 200nm respectively. For all z, a minimum is reached at w = 400nm, a width corresponding to a propagating mode in the Si waveguide with an effective index of 2.3 matching that of the InP-based wire where the cavity is etched. This phase-matching enables the maximum transfer of light and thus the minimum Q_c.

The unloaded quality factor Q_0 is obtained by fitting the L-L curve with standard rate equations for QW lasers [32]:

$$\frac{dS}{dt} = \frac{-S}{\tau_{ph}} + \Gamma\sigma v_g (N - N_{tr})S + \Gamma\beta BN^2$$

#144421 - $15.00 USD Received 18 Mar 2011; revised 19 Apr 2011; accepted 19 Apr 2011; published 26 Apr 2011

$$\frac{dN}{dt} = -\frac{N}{\tau_{nr}} - BN^2 + \sigma v_g (N - N_{tr})S + R$$

where S is the photon density, N the carrier density, N the carrier density, τ_{ph} the photon lifetime, β the spontaneous emission factor, B the bimolecular radiative recombination coefficient, τ_{nr} the non-radiative carrier relaxation time and R the pumping rate proportional to the optical pump fluence. τ_{ph} is linked to τ_0 and τ_c by the relation $1/\tau_{ph} = (1/\tau_0 + 1/\tau_c)/2$. Γ and v_g are fixed to 0.25 and 10^8 m.s^{-1} respectively, determined using 3D FDTD calculations [20]. From literature [33], we take $N_{tr} = 10^{18}$cm^{-3} and B = 3.10^{10}cm^3.s^{-1}; τ_{nr} is measured to be 200ps [34]. In order to fit the rate equation, we introduce a condition on the differential gain:

$$\sigma = \frac{2}{\Gamma v_g N_{tr}} \left(\frac{1}{\tau_c} \frac{P_0}{2(P_1 - P_0)} - \frac{1}{\tau_0} \right)$$

where P_1 is the pump power when the transmission at resonance equals to 1. Finally, β is left as a free variable. The result of the fit using this model is plotted on Fig. 2a together with the measurement values. Excellent fits of the measurements are obtained for τ_0 ranging from 10ps to 83ps ($6100<Q_0<50000$) and $0.16<\beta<0.35$.

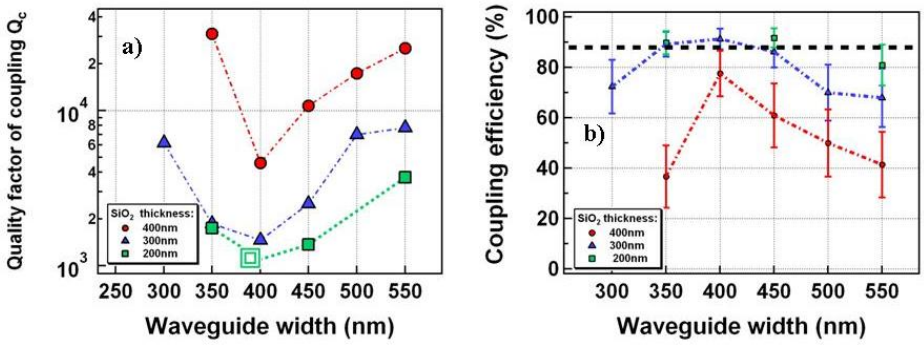

Fig. 5. Characteristic coupling figures. a) Measured quality factor associated to the evanescent wave coupling (Q_c) for various SOI waveguide width w and for 3 low-index layer thicknesses. b) Coupling efficiency of the emitted light into the SOI wire as a function of the structure parameters. The uncertainty on the coupling efficiency is plotted on the figure with segments. We indicate by the black dotted line the estimated boundary in terms of coupling efficiency between lasing and non lasing structures.

To improve the estimates, these values are cross-checked with the results of the fit of a L-L curve for the same cavity but coupled to a waveguide of different width. We obtain $16.5ps<\tau_0<49.5ps$ ($10000<Q_0<30000$) and $0.2<\beta<0.3$ which are typical for this type of nanolasers allowing low laser threshold and ultrafast dynamics [35]. Even though it is not possible to determine τ_0 precisely, this method is preferred to the usual way of finding the Q factor by measuring the laser spectral linewidth at threshold, as the linewidth of a semiconductor laser is not simply fixed by the optical losses in the system but depends on the pump duration, the phase-amplitude coupling and various sources of noise [36]. However, our results give us sufficient information on the total losses of the system to determine the coupling efficiencies of the nanolasers to the SOI wires.

The coupling efficiency, η, of the emitted light into the Si wires is plotted for the different studied structures in Fig. 5b. Each segment represents the possible range of values for η taking into account the uncertainties in Q_0. By adjusting the parameters of the structures we demonstrate it is possible to vary the efficiency at will from around 20% to more than 90% by

#144421 - $15.00 USD Received 18 Mar 2011; revised 19 Apr 2011; accepted 19 Apr 2011; published 26 Apr 2011

controlling the evanescent wave coupling strength, i.e. Q_c. As expected, the maximum of efficiency is obtained for the thinnest low-n layer and for w = 400nm which gives the smallest value of Q_c. Yet, the cases corresponding to the highest η do not necessarily correspond to the ideal configuration as it also gives the largest optical losses in the system which may result in an increase of the laser threshold or even worse in a non-lasing situation. The transition from lasing to non-lasing structures is observed to occur when the coupling efficiency goes beyond 88%, when the total Q factor of the system is lower than 2000. This estimated boundary between the two regimes is indicated by the dotted line on Fig. 5b. Of course further improvement of the intrinsic quality factor of the cavities would permit us to obtain larger Q_0/Q_c ratios, i.e. larger coupling efficiencies while maintaining sufficiently small total losses to observe laser emission. As demonstrated, Q_c can be adjusted by changing the structure parameters in order to obtain optimal coupling of laser emission to the SOI waveguide which can lead to coupling efficiencies well beyond 90%.

5. Conclusion and discussion

The concept of hybrid III-V semiconductor/silicon photonics has been brought forward to nanophotonic world by the integration of InP-based PhC nanolasers on SOI single mode waveguides. We have demonstrated the most compact lasers integrated on a Si optical circuits with low thresholds and within the telecom window. This system has many assets in terms of performance and for future applications. Indeed, taking advantage of the quasi perfect confinement of light within PhCs, we have fabricated lasers with $5\mu m^2$ footprints which correspond to at least an order of magnitude reduction over previously demonstrated hybrid systems. The breakthrough result in this work is that almost all the emitted light is useful as it is efficiently coupled into the subjacent Si waveguides and thus can be further used directly in a CMOS compatible dense nanophotonic networks of interconnects adapted for computer-com.

The highly efficient evanescent wave coupling was obtained by tailoring the optical properties of both the SOI waveguide and the III-V nanocavity and through the fine control over the technological processing of the structure such as the precise lithographic positioning of the nanocavity with respect to the SOI wires.

Until now, the practical use of PhCs in an integrated photonic circuit has been an extremely challenging task. Establishing the communication between active nanodevices and the outside world, whilst mastering optical losses and photonic functionalities has been a major problem. To the best of our knowledge, two solutions have been proposed in the literature: the first one consists in using a tapered optical fibre to extract the light from the PhC [37,38]. This approach, obviously limited to one isolated element presents also limitations in terms of coupling due to the large difference in refractive index between the optical fibre and the III-V semiconductor and the imprecise control of the of the fibre-cavity distance. The other possibility is an all III-V semiconductor based approach as for telecom devices, making use of epitaxial regrowth to separate the active regions where the lasers are made from the passive ones where light propagates without being absorbed [39,40]. Compared to the hybrid approach, this type of structure suffers from the lack of direct compatibility with CMOS electronics as they are made in a different platform. Moreover, this all III-V semiconductor solution relies on the use of suspended membranes to form the high index contrast waveguide necessary for the vertical confinement in PhC devices which is an evident drawback for mechanical reliability.

The III-V/SOI hybrid system reported here brings an efficient and elegant solution for making use of active PhCs within a photonic circuit combining the best of III-V semiconductor and Si photonics. The remaining obstacle to the use of PhC nanolasers with CMOS electronics is the electrical injection which is necessary for electro-optical conversion. Recent progress on this subject consists of either creating a lateral p-i-n junction [41] or smartly designing the electrical contacts [42]. These are encouraging approaches which could be implemented also within our hybrid system.

#144421 - $15.00 USD Received 18 Mar 2011; revised 19 Apr 2011; accepted 19 Apr 2011; published 26 Apr 2011

Acknowledgments

A.B. and Y. H. contributed equally to make this work successful and would both deserve to be first author. The authors acknowledge for funding FP7 HISTORIC European Project and ANR Jeunes chercheurs French National project PROWOC. The SOI wafers were fabricated within the ePIXfab European silicon platform. We thank Remy Braive for his help in the etching of photonic crystals and Bjorn Maes for useful discussion.

#144421 - $15.00 USD Received 18 Mar 2011; revised 19 Apr 2011; accepted 19 Apr 2011; published 26 Apr 2011